Metabolism Clinical and Experimental 93 (2019) 33–43

Contents lists available at ScienceDirect

Metabolism Clinical and Experimental

journal homepage: www.metabolismjournal.com

Hyperinsulinemia drives hepatic insulin resistance in male mice with liver-specific *Ceacam1* deletion independently of lipolysis

Hilda E. Ghadieh [a,b], Lucia Russo [b], Harrison T. Muturi [a], Simona S. Ghanem [b], Iyad H. Manaserh [b], Hye Lim Noh [c], Sujin Suk [c], Jason K. Kim [c,d], Jennifer W. Hill [b], Sonia M. Najjar [a,b,e,*]

[a] Department of Biomedical Sciences, Heritage College of Osteopathic Medicine, Ohio University, Athens, OH, USA
[b] Center for Diabetes and Endocrine Research, College of Medicine and Life Sciences, University of Toledo, Toledo, OH, USA
[c] Program in Molecular Medicine, University of Massachusetts Medical School, Worcester, MA, USA
[d] Division of Endocrinology, Metabolism and Diabetes, University of Massachusetts Medical School, Worcester, MA, USA
[e] Diabetes Institute, Heritage College of Osteopathic Medicine, Ohio University, Athens, OH, USA

ARTICLE INFO

Article history:
Received 19 November 2018
Accepted 16 January 2019

Keywords:
Hyperinsulinemia
Insulin clearance
Insulin resistance
Hyperphagia
Fatty acid synthase
Energy balance

ABSTRACT

Background: CEACAM1 regulates insulin sensitivity by promoting insulin clearance. Accordingly, global C57BL/6J. *Cc1*$^{-/-}$ null mice display hyperinsulinemia due to impaired insulin clearance at 2 months of age, followed by insulin resistance, steatohepatitis, visceral obesity and leptin resistance at 6 months. The study aimed at investigating the primary role of hepatic CEACAM1 in insulin and lipid homeostasis independently of its metabolic effect in extra-hepatic tissues.

Methods: Liver-specific C57BL/6J.*AlbCre*+*Cc1*$^{fl/fl}$ mice were generated and their metabolic phenotype was characterized by comparison to that of their littermate controls at 2–9 months of age, using hyperinsulinemic-euglycemic clamp analysis and indirect calorimetry. The effect of hyperphagia on insulin resistance was assessed by pair-feeding experiments.

Results: Liver-specific *AlbCre*+*Cc1*$^{fl/fl}$ mutants exhibited impaired insulin clearance and hyperinsulinemia at 2 months, followed by hepatic insulin resistance (assessed by hyperinsulinemic-euglycemic clamp analysis) and steatohepatitis at ~ 7 months of age, at which point visceral obesity and hyperphagia developed, in parallel to hyperleptinemia and blunted hypothalamic STAT3 phosphorylation in response to an intraperitoneal injection of leptin. Hyperinsulinemia caused hypothalamic insulin resistance, followed by increased fatty acid synthase activity, which together with defective hypothalamic leptin signaling contributed to hyperphagia and reduced physical activity. Pair-feeding experiment showed that hyperphagia caused systemic insulin resistance, including blunted insulin signaling in white adipose tissue and lipolysis, at 8–9 months of age.

Conclusion: *AlbCre*+*Cc1*$^{fl/fl}$ mutants provide an in vivo demonstration of the key role of impaired hepatic insulin clearance and hyperinsulinemia in the pathogenesis of secondary hepatic insulin resistance independently of lipolysis. They also reveal an important role for the liver-hypothalamic axis in the regulation of energy balance and subsequently, systemic insulin sensitivity.

1. Introduction

Insulin clearance occurs mostly in the liver and to a lower extent in kidneys and other peripheral tissues [1]. Upon its pulsatile release from pancreatic β-cells into the portal vein [2,3], insulin crosses the sinusoidal endothelium to reach and activate its receptor on the hepatocytic surface membrane [4]. This phosphorylates other substrates and delivers insulin to early/late endosomes for degradation before the receptor recycles back to the surface membrane [5]. In this manner, excess insulin is rapidly removed and maintained at a physiologically higher concentration in the portal vein than in the systemic circulation [6]. Under hyperinsulinemic conditions, the receptor is diverted to lysosomal degradation [7,8] to cause cellular insulin resistance.

Chronic hyperinsulinemia also induces hepatic de novo lipogenesis by activating SREBP1c, a master transcriptional regulator of lipogenic genes [9]. Thus, impaired hepatic insulin clearance leads to a concomitant increase in hepatic steatosis and hepatic insulin resistance.

Abbreviations: *AlbCre*+*Cc1*$^{fl/fl}$, Mice with liver-specific deletion of *Ceacam1* gene; *AlbCre–Cc1*$^{+/+}$, Wild-type controls; *AlbCre*+*Cc1*$^{+/+}$, Albumin-Cre controls; *AlbCre–Cc1*$^{fl/fl}$, *Ceacam1*-floxed controls; FASN, Fatty acid synthase; IR$_\beta$, β subunit of the insulin receptor; NEFA, Non-esterified fatty acids; POMC, Pro-opiomelanocortin; STAT3, Signal transducer and activator of transcription 3; WAT, White adipose tissue.

* Corresponding author at: Department of Biomedical Sciences, Heritage College of Osteopathic Medicine, Irvine Hall, 1 Ohio University, Athens, OH 45701-2979, USA.
E-mail address: najjar@ohio.edu (S.M. Najjar).

https://doi.org/10.1016/j.metabol.2019.01.008
0026-0495/

Carcinoembryonic antigen-related cell adhesion molecule 1 (CEACAM1), a surface membrane substrate of the insulin receptor, promotes insulin clearance [10,11] by taking part of the insulin-insulin receptor complex and increasing its rate of uptake and endosomal targeting [12,13]. Subsequently, it binds to cytosolic fatty acid synthase (FASN), an event that detaches it from the complex to facilitate the dissociation of insulin from its receptor while mediating an inhibitory effect of insulin on FASN [14]. This restricts hepatic de novo lipogenesis and protects the liver against high portal insulin levels. Consistently, mice with null deletion of *Ceacam1* gene (*Cc1*$^{-/-}$) manifested impaired insulin clearance and chronic hyperinsulinemia at 2 months, followed by insulin resistance, primarily hepatic, at ~6 months of age when propagated on C57BL/6J background [11]. Deletion of *Ceacam1* gene induced triacylglycerol production and redistribution to white adipose tissue (WAT). This resulted in hepatic steatosis and visceral obesity at 2 months, followed by lipolysis and mobilization of non-esterified free fatty acids (NEFA) at ~6 months of age [11].

Because of the regulatory effect of CEACAM1 on lipid production (by preventing hyperinsulinemia or mediating insulin downregulation of FASN activity), it is possible that deleting *Ceacam1* primarily increased FASN synthesis and hepatic de novo lipogenesis, independently of hyperinsulinemia, to lead to visceral obesity and NEFA mobilization, which causes hepatic insulin resistance (portal hypothesis) [15] that in turn induces a compensatory increase in insulin secretion and ensuing hyperinsulinemia. This model would be consistent with the commonly accepted paradigm of primary insulin resistance causing chronic hyperinsulinemia mainly by inducing a compensatory increase in insulin secretion. However, blocking lipolysis with nicotinic acid did not restore insulin clearance or sensitivity [16]. Together with intact β-cell mass [11], this indicates that hyperinsulinemia in *Cc1*$^{-/-}$ mice resulted primarily from impaired insulin clearance rather than increased insulin secretion, and that it caused insulin resistance independently of lipolysis.

Cc1$^{-/-}$ mice also developed leptin resistance concomitantly with insulin resistance, basal hyperphagia and decreased spontaneous locomotor activity [17]. Whereas hyperinsulinemia-driven insulin resistance in the hypothalamus caused energy imbalance, as shown by liver-specific rescuing of *Ceacam1* in *Cc1*$^{-/-}$ mice [16], deleting CEACAM1 from the arcuate nucleus region of the hypothalamus, in particular pro-opiomelanocortin (POMC)-expressing neurons, may contribute to the regulation of energy imbalance in *Cc1*$^{-/-}$ mutants [17].

Given the multiple factors that could contribute to insulin resistance in *Cc1*$^{-/-}$ mice, including impaired insulin clearance, lipolysis and leptin resistance, it became imperative to identify its primary underlying mechanism with the overarching goal to determine whether it caused or resulted from hyperinsulinemia. To this end, we generated a liver-specific C57BL/6J.*Ceacam1* knockout mouse (*AlbCre*+*Cc1*$^{fl/fl}$) and characterized the hepatic and extra-hepatic mechanisms that could be implicated in its altered metabolic phenotype.

2. Methods

2.1. Generation of Liver-specific AlbCre +Cc1$^{fl/fl}$ Mice

As in the conditional T cell-specific null mouse [18], the targeting construct inserted a loxP-neo cassette in intron 6 and a loxP fragment in intron 9, deleting a sequence that encodes the cytoplasmic domain [19]. We crossed *Cc1*$^{loxp/loxp}$ mice with transgenic mice expressing Cre under the transcriptional control of the albumin gene promoter (*AlbCre*) on C57BL/6J background (Jackson Laboratories, Bar Harbor, ME) (Fig. S1). Heterozygotes were backcrossed >6× with C57BL/6J mice. Offsprings were genotyped by PCR analysis of ear DNA, using primers shown in Fig. S1. As controls, we used homozygotes with wild-type *Ceacam1* allele with (*AlbCre*+*Cc1*$^{+/+}$) or without *AlbCre* (*AlbCre*–*Cc1*$^{+/+}$), and homozygotes with *Ceacam1*-floxed allele, without *AlbCre* (*AlbCre*–*Cc1*$^{fl/fl}$); all from the same breeding to rule out potential confounding effects of floxing and introducing *AlbCre*.

All animals were housed in a 12 h-dark/light cycle and fed standard chow (Harlan Teklad 2016; Harlan, Haslett, MI) ad libitum. All procedures and animal experiments were approved by the Animal Care and Utilization Committee of each institution.

2.2. Body Composition

Body composition was assessed by nuclear magnetic resonance technology (Bruker Minispec; Billerica, MA).

2.3. Indirect Calorimetry

Awake mice ($n = 4$/genotype) were individually caged (CLAMS system, Columbus Instruments, Columbus, OH) over a 3 day-period after being acclimated for 2 days [17]. Mice had access to food and water ad libitum. Spontaneous physical activity was measured on the *x* axis (locomotor), *y* axis (ambulatory), and *z* axis (standing). Total activity was calculated as the average of x/y/z activities. Oxygen consumption (VO_2), CO_2 production (VCO_2), and heat generation were sampled every 20 min and normalized to fat-free lean mass. The respiratory exchange rate was calculated as the VCO_2/VO_2 ratio. Data were represented as mean ± SEM of light (700–1900 h) and dark (1900 to 700 h) cycles.

2.4. Glucose and Insulin Tolerance Tests

Awake mice were fasted for 6–7 h before being subjected to intraperitoneal dextrose and insulin injections, and blood glucose was measured from the tail at each time point at 0–180 min post-injection [16].

2.5. Hyperinsulinemic-euglycemic Clamp Analysis

A 2-h hyperinsulinemic-euglycemic clamp was performed in awake overnight-fasted mice with primed and continuous infusion of human regular insulin (Humulin, Lilly, Indianapolis, IN) at a rate of $2.5 mU x kg^{-1} x min^{-1}$ [11]. Glucose metabolism was estimated with a continuous infusion of 0.05 μCi/min of [3−^{3}H] glucose (PerkinElmer and Analytical Sciences, Hopkinton, MS) and subsequently with 0.1 μCi/min throughout the clamp.

2.6. Biochemical Parameters

Retro-orbital venous blood was drawn at 1100 h from overnight fasted mice and plasma was analyzed by ELISA for insulin, C-peptide (ALPCO, Salem, NH), and adiponectin (Abcam, Cambridge, MA). Plasma NEFA and triacylglycerol were assayed by enzymatic colorimetric assays from Wako (Richmond, VA) and Pointe Scientific (Canton, MI), respectively, and hepatic triacylglycerol were assayed as previously described [11].

Mice were fasted 6–7 h before leptin and glucagon were assayed by ELISA kits from ALPCO and R&D Systems (Minneapolis, MN), respectively.

2.7. Isolation of Primary Hepatocytes

Primary hepatocytes were isolated by perfusing livers (1 mL/min) of anesthetized mice with Collagenase-Type II (1 mg/mL) (Worthington, Lakewood, NJ), and plated in 6-well plates in complete Williams-E medium at 1×10^6 cells/well [10].

2.8. Biotin Labeling

Primary cells were incubated in the absence or presence of 100 nM insulin (Sigma-Aldrich, Saint Louis, MO) at 37 °C for 5 min, followed

by incubation on ice with biotin (1 mg/mL) (Pierce, Rockford, IL) in PBS for 30 min [16]. Cells were lysed in 1%Triton-X and proteins immunoprecipitated with streptavidin (Fisher Scientific, Waltham, MA), and immunoblotted with 1:1000 of insulin receptor alpha (IR_α) antibody (N-20, Santa Cruz) or a custom-made mouse Ab3759 polyclonal antibody against CEACAM1 [20], followed by horseradish peroxidase-conjugated mouse anti-rabbit IgG antibody (Jackson Immunoresearch, West Grove, PA) and enhanced chemiluminescence (ECL, Amersham Pharmacia, Sunnyvale, CA).

2.9. Insulin Internalization

Human [^{125}I]-Insulin (PerkinElmer Life Sciences, Akron, OH) (30,000 cpm) was allowed to bind to primary hepatocytes at 4 °C for 5 h in Krebs-Ringer phosphate (KRP) buffer [16], before unbound insulin was removed, and surface-bound insulin was collected in acidic PBS (pH 3.5). Cells were washed and lysed with 0.4 N NaOH to account for cell-associated internalized insulin. Internalized insulin was calculated as percent cell-associated per specifically bound ligand (the sum of surface-bound plus cell-associated ligand).

2.10. Ex-vivo Palmitate Oxidation

Liver homogenate was added to 1 mL of solution A [0.2 mM of [$^{1\text{-}14}$C]-palmitate (0.5 mCi/mL) (American Radiolabeled Chemicals Inc., St Louis, MO)-2 mM ATP] and left at 30 °C for 45 min in a sealed beaker [21]. Benzothonium hydroxide (Sigma-Aldrich) was added to a basket attached to the beaker and the reaction was terminated with perchloric acid to recover trapped CO_2 radioactivity and the partial oxidation products to be measured by liquid scintillation in CytoCint (MP Biomedicals, Solon, OH). The oxidation rate was expressed as the sum of total and partial fatty acid oxidation in nmoles/g/min.

2.11. Fatty Acid Synthase Activity

Livers were homogenized, centrifuged and the supernatant added to a reaction mix containing 0.1 μCi [^{14}C]-malonyl-CoA (Perkin-Elmer) and 25 nmol malonyl-CoA in the absence or presence of 500 μM NADPH (Sigma-Aldrich) [14]. The reaction was stopped with 1:1 chloroform:methanol solution and samples were centrifuged, butanol-extracted and counted. FASN enzymatic activity was calculated as cpm of [^{14}C]-incorporated Bq/μg cell lysates.

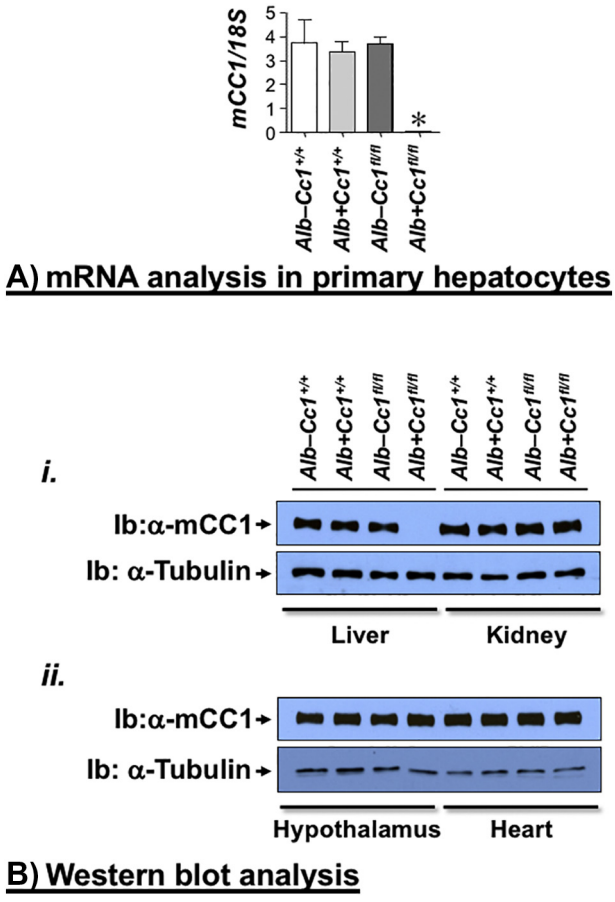

Fig. 1. Tissue-specific expression of mouse CEACAM1 (mCC1). (A) Primary hepatocytes from *Alb–Cc1*$^{+/+}$ (white bar), *Alb+Cc1*$^{+/+}$ (light grey bar), *Alb–Cc1*$^{fl/fl}$ (dark grey bar) and *Alb+Cc1*$^{fl/fl}$ (black bar) were isolated and analyzed by qRT-PCR in triplicate to assess mouse *Ceacam1* mRNA level. Values are expressed as mean ± SEM; *$P < 0.05$ vs *Alb–Cc1*$^{+/+}$, *Alb+Cc1*$^{+/+}$ and *Alb–Cc1*$^{fl/fl}$. (B) Western blot analysis of mouse (mCC1) CEACAM1 protein content in (*i*) liver and kidney, and (*ii*) hypothalamus and heart was performed by immunoblotting (Ib) the upper portion of the blot with a polyclonal antibody against CEACAM1 (α-CC1) and the lower portion with α-Tubulin to normalize for protein loading. Gels represent more than two experiments (different mice/genotype).

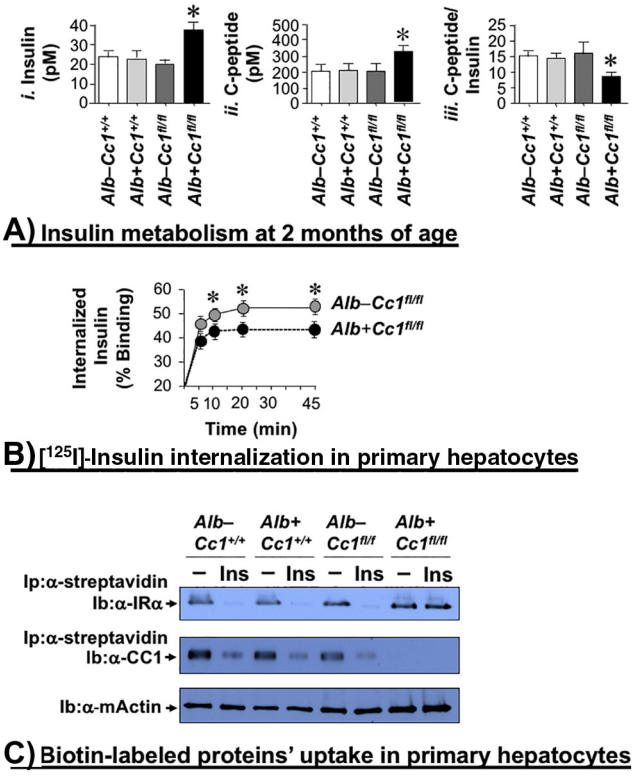

Fig. 2. Analysis of insulin clearance. (A) *Alb–Cc1*$^{+/+}$ (white bar), *Alb+Cc1*$^{+/+}$ (light grey bar), *Alb–Cc1*$^{fl/fl}$ (dark grey bar) and *Alb+Cc1*$^{fl/fl}$ (black bar) ($n = 5$/genotype; 2-month-old) were fasted overnight and retro-orbital blood was drawn to assess plasma insulin (*i*) and C-peptide (*ii*) levels to calculate steady-state C-peptide/insulin molar ratio (*iii*) as a measure of insulin clearance. Assays were performed in triplicate. Values are expressed as mean ± SEM; *$P < 0.05$ vs *Alb–Cc1*$^{+/+}$, *Alb+Cc1*$^{+/+}$ and *Alb–Cc1*$^{fl/fl}$. (B) [^{125}I]-insulin internalization was measured in triplicate as percent of specifically-bound ligand in primary hepatocytes from *Alb–Cc1*$^{fl/fl}$ (dark grey circles) and *Alb+Cc1*$^{fl/fl}$ (black circles). $n = 6$ mice/genotype. *$P < 0.05$ vs *Alb+Cc1*$^{fl/fl}$. (C) Cell surface proteins in primary hepatocytes treated with buffer (−) or insulin (Ins) and then labeled with biotin. Proteins were immunoprecipitated (Ip) with α-streptavidin beads prior to analysis by 7% SDS-PAGE and immunoblotting (Ib) with antibodies against IR_α and mouse CEACAM1. Total lysates were also analyzed by immunoblotting with mouse Actin antibody (α-mActin) to normalize against total loaded proteins. Gels represent more than two experiments (different mice/genotype/experiment).

2.12. Daily Food Intake and Pair-feeding

The average daily food intake was assessed in individually caged mice over a 5-day-period. Based on the average daily food intake of individually caged 8-month-old mice over a 5-day-period, mutants were subjected to a pair-feeding regimen: 2.5 g food/day (0.5 g less than the ad libitum-fed mutants) for the first week [22]. Because this feeding program prevented weight gain, the amount of food was increased to 3.0 g/day as opposed to 5.0 g of food/day to the ad libitum-fed group in the second week, and insulin tolerance was assessed.

2.13. Hypothalamic Leptin Signaling

Mice ($n = 3$–5/treatment/genotype) were injected intraperitoneally with vehicle (Veh, open or solid bars) or leptin (Lep, grey- and black-striped bars) 45 min prior to tissue isolation [17]. Coronal sections from the medial hypothalamus were subjected to immunohistochemical analysis with phospho-STAT3 antibody (rabbit polyclonal antiserum, Cell Signaling Technologies, Beverly, MA). Images of stained hypothalamic neurons of the medial hypothalamus were counted using Open CFU [23].

2.14. Western Blot Analysis

Tissue lysates were analyzed by immunoprobing with custom-made rabbit polyclonal Ab3759 against the mouse CEACAM1 extracellular domain [24], and phosphorylated CEACAM1 (α-pCEACAM1) (Bethyl Laboratories, Montgomery, TX) [25,26]. Antibodies against phospho-insulin receptor β (pIR$_\beta$) (phospho-Y1361), IR$_\beta$ (C18C4) (Abcam), FASN, phospho-Akt^{Ser473} and Akt (Cell Signaling) were also used. α-Tubulin monoclonal antibody (Cell Signaling) was used for normalization. Blots were incubated with horseradish peroxidase-conjugated donkey anti-rabbit IgG antibody or anti-mouse IgG antibody (GE Healthcare Life Sciences, Amersham), and detected by ECL.

2.15. Quantitative Real-time-PCR (qRT-PCR)

Total RNA was isolated with PerfectPure RNA Tissue Kit (Fisher Scientific, Waltham, MA). cDNA was synthesized by iScript cDNA Synthesis Kit (Bio-Rad), using 1 μg of total RNA and oligodT primers (Table S1). cDNA was evaluated with qRT-PCR (StepOne Plus, Applied Biosystems, Foster City, CA), and mRNA was normalized to *Gapdh* [21].

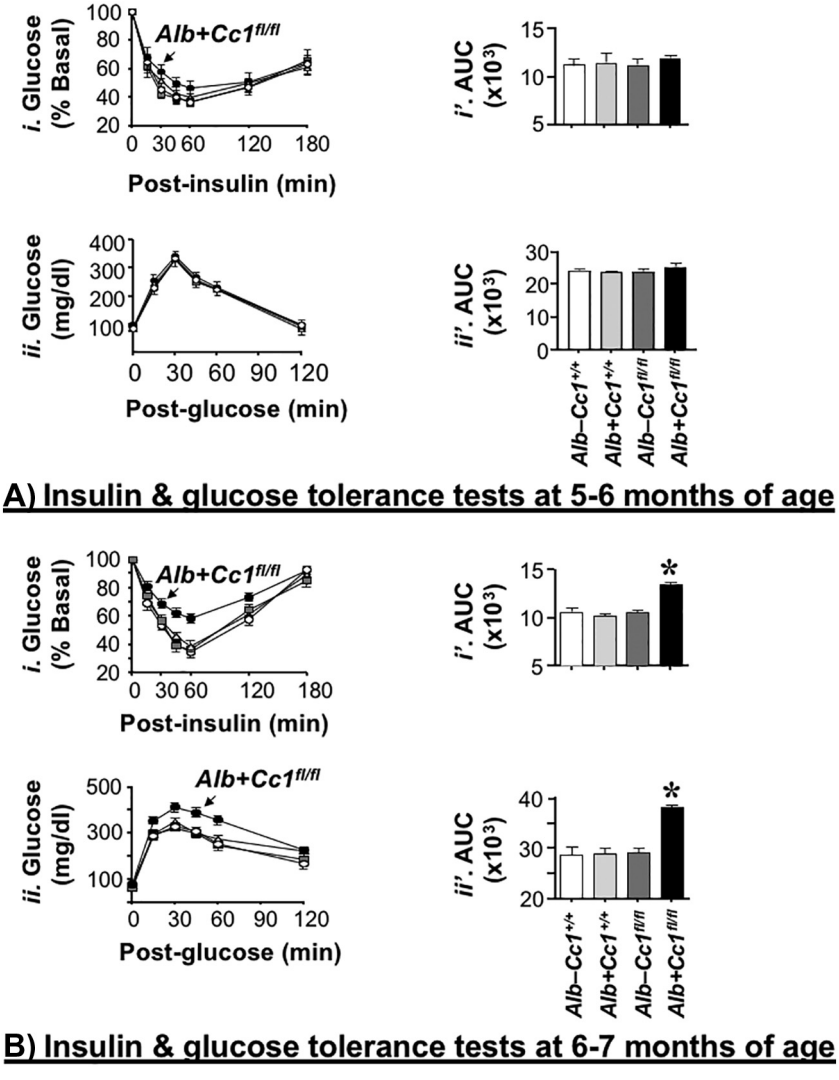

Fig. 3. Insulin and glucose tolerance tests. 7 h-fasted mice at (A) 5–6 and (B) 6–7 months of age ($n = 7$–8/genotype) were injected intraperitoneally with insulin or glucose to assess insulin (*i*) and glucose (*ii*) tolerance, respectively. Accompanying graphs represent the area under the curve (AUC) (*i*' and *ii*'). *Alb–Cc1*$^{+/+}$ (white circles and bars), *Alb+Cc1*$^{+/+}$ (light grey triangles and bars), *Alb–Cc1*$^{fl/fl}$ (dark grey squares and bars) and *Alb+Cc1*$^{fl/fl}$ (black circles and bars). Values are expressed as mean ± SEM. *$P < 0.05$ vs *Alb–Cc1*$^{+/+}$, *Alb+Cc1*$^{+/+}$ and *Alb–Cc1*$^{fl/fl}$.

2.16. Statistical Analysis

Data were analyzed using one-way ANOVA analysis with Bonferroni correction or two-tailed Student *t*-test using GraphPad Prism6 software. Data were presented as mean ± SEM. $P < 0.05$ was considered statistically significant.

3. Results

3.1. Liver-specific Deletion of CEACAM1

qRT-PCR analysis demonstrated that mouse *Ceacam1* mRNA (m*Cc1*) was absent in primary hepatocytes from *AlbCre+Cc1*$^{fl/fl}$ mice (*Alb+Cc1*$^{fl/fl}$ for simplicity) (Fig. 1A). Immunoblotting with mouse α-CEACAM1 (Ib:α-mCC1) detected CEACAM1 protein in the livers of controls (*Alb–Cc1*$^{+/+}$, *Alb+Cc1*$^{+/+}$ and *Alb–Cc1*$^{fl/fl}$), but not *Alb+Cc1*$^{fl/fl}$ mutants (Fig. 1B.*i*). CEACAM1 protein content was intact in other tissues from mutant mice, including kidney, hypothalamus and heart (Fig. 1B.*i-ii*).

3.2. Early Onset of Impaired Insulin Clearance and Hyperinsulinemia in *Alb+Cc1*$^{fl/fl}$ Mice

Like *Cc1*$^{-/-}$ [11], *Alb+Cc1*$^{fl/fl}$ exhibited hyperinsulinemia at 2 months of age (Fig. 2A.*i*) in parallel to impaired insulin clearance, as indicated by steady-state C-peptide/insulin molar ratio (Fig. 2A.*iii*). Consistent with increased rate of receptor-mediated insulin endocytosis by phosphorylated CEACAM1 [12], [^{125}I]-insulin internalization was significantly reduced ($P < 0.05$) in primary hepatocytes isolated from *Alb+Cc1*$^{fl/fl}$ (black circles) by comparison to hepatocytes from *Alb–Cc1*$^{fl/fl}$ controls (dark grey circles) (Fig. 2B). In addition, immunoblotting the biotin-streptavidin immunopellet (Ip) with polyclonal antibodies against IR$_\alpha$, the extracellular subunit of the insulin receptor (IR), and mouse CEACAM1 (Fig. 2C) revealed insulin-induced IR$_\alpha$ and CEACAM1 internalization, measured by the loss of biotin-labeled surface membrane proteins in insulin (Ins)- versus buffer-treated hepatocytes [10] in control groups but not in *Alb+Cc1*$^{fl/fl}$ mice. Lower insulin (Fig. 2B) and biotin-labeled IR$_\alpha$ (Fig. 2C) internalization in *Alb+Cc1*$^{fl/fl}$ hepatocytes demonstrated defective targeting of the insulin-insulin receptor complex to the degradation process in the absence of CEACAM1, an event that could impair insulin clearance.

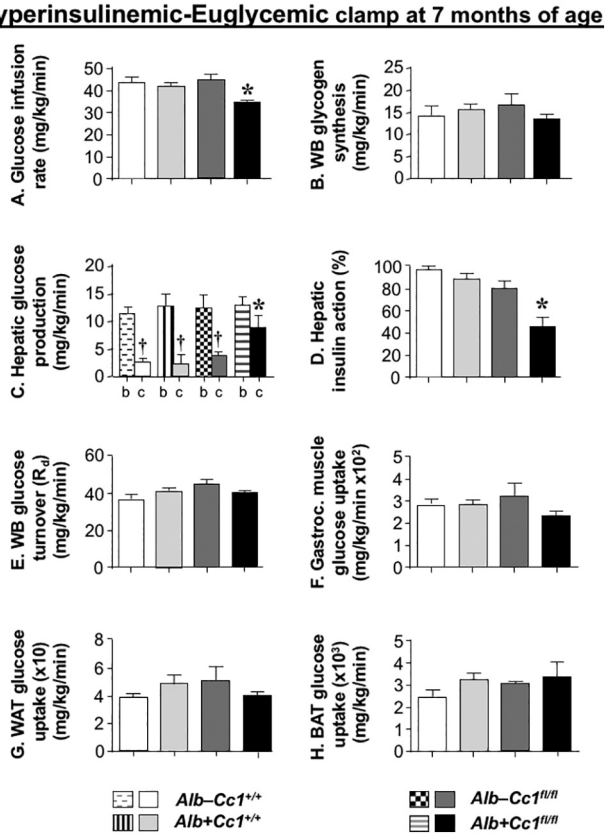

Fig. 4. Hyperinsulinemic–euglycemic clamp analysis performed on 7-month-old awake overnight-fasted mice. Measurements under clamp conditions with primed and continuous infusion of insulin are shown for *Alb–Cc1*$^{+/+}$ (white bar), *Alb+Cc1*$^{+/+}$ (light grey bar), *Alb–Cc1*$^{fl/fl}$ (dark grey bar) and *Alb+Cc1*$^{fl/fl}$ (black bar) mice. In (C), measurements for the basal (b) and clamp (c) conditions are also shown. The data are cumulative of 2 sets of experiments performed on different sets of mice at the same age. ($n = 5$ for *Alb–Cc1*$^{+/+}$, $n = 12$ for *Alb+Cc1*$^{+/+}$ and *Alb–Cc1*$^{fl/fl}$ and $n = 20$ for *Alb+Cc1*$^{fl/fl}$). Values are expressed as mean ± SEM; *$P < 0.05$ vs *Alb–Cc1*$^{+/+}$, *Alb+Cc1*$^{+/+}$ and *Alb–Cc1*$^{fl/fl}$; †$P < 0.05$ vs basal (b).

3.3. *Alb+Cc1*$^{fl/fl}$ Mice Developed Secondary Hepatic Insulin Resistance at 6–7 Months of Age

Up to 5–6 months of age, *Alb+Cc1*$^{fl/fl}$ mutants displayed normal glucose clearance in response to intraperitoneal injections of insulin

Table 1
Plasma and tissue biochemistry in mice at 6–7 months of age.

	Alb–Cc1$^{+/+}$	*Alb+Cc1*$^{+/+}$	*Alb–Cc1*$^{fl/fl}$	*Alb+Cc1*$^{fl/fl}$
Body Weight (g)	30.1 ± 0.5	31.2 ± 0.5	31.4 ± 0.5	36.9 ± 0.9*,†,‡
% Fat Mass	6.2 ± 0.5	6.1 ± 0.2	6.5 ± 0.3	9.7 ± 0.3*,†,‡
% Lean Mass	51.4 ± 1.2	52.7 ± 1.5	52.8 ± 1.5	46.4 ± 1.2*,†,‡
% WAT/BW	2.2 ± 0.1	2.2 ± 0.2	2.0 ± 0.4	3.5 ± 0.4*,†,‡
NEFA (mEq/L)	0.4 ± 0.0	0.7 ± 0.0	0.7 ± 0.0	0.8 ± 0.1
Insulin (pmol/L)	32.3 ± 1.4	34.1 ± 1.5	36.7 ± 1.5	56.1 ± 1.7*,†,‡
C-peptide (pmol/L)	242 ± 34	271 ± 42	255 ± 39	575 ± 50*,†,‡
C/I molar ratio	9.8 ± 1.4	9.5 ± 1.2	9.8 ± 1.7	6.5 ± 1.9*,†,‡
Glucagon (pg/mL)	65.7 ± 5.4	67.1 ± 4.9	63.8 ± 5.2	69.8 ± 6.1
Triacylglycerol (TG, mg/dL)	51.1 ± 2.7	49.1 ± 4.2	48.2 ± 5.1	52.7 ± 4.5
Hepatic TG (μg/mg protein)	66.2 ± 5.4	64.1 ± 4.3	62.3 ± 2.9	88.2 ± 3.4*,†,‡
Fast blood glucose (mg/dL)	78 ± 2	80 ± 2	79 ± 2	85 ± 2
Fed blood glucose (mg/dL)	131 ± 2	126 ± 2	129 ± 3	158 ± 3*,†,‡
Leptin (ng/mL)	3.1 ± 0.1	3.1 ± 0.2	3.2 ± 0.1	10.4 ± 0.3*,†,‡
Adiponectin (ng/mL)	33.6 ± 0.9	31.8 ± 1.2	32.4 ± 1.3	26.2 ± 0.8*,†,‡

Male mice (6–7 months of age, $n \geq 6$/genotype) were fasted overnight (except for leptin and glucagon when mice were fasted for 6–7 h) before blood was drawn and tissues were excised. Values refer to plasma levels, unless otherwise mentioned. Values are expressed as mean ± SEM. WAT: White adipose tissue; BW: Body weight; C/I: C-peptide/Insulin molar ratio as measure of insulin clearance; NEFA: Non-esterified fatty acid; TG: Triacylglycerol.

* $P < 0.05$ vs *AlbCre–Cc1*$^{+/+}$.

† $P < 0.05$ vs *AlbCre+Cc1*$^{+/+}$.

‡ $P < 0.05$ vs *AlbCre–Cc1*$^{fl/fl}$.

(Fig. 3A.*i*, black circles, black bars) and glucose (Fig. 3A.*ii*) relative to their three controls [*Alb–Cc1*$^{+/+}$ (white circles and bars), *Alb+Cc1*$^{+/+}$ (light grey triangles and bars) and *Alb–Cc1*$^{fl/fl}$ (dark grey squares and bars)]. At 6–7 months; however, *Alb+Cc1*$^{fl/fl}$ mutants exhibited intolerance to exogenous insulin (Fig. 3B.*i*) and glucose (Fig. 3B.*ii*), as supported by the ~2-fold higher area under the curve (AUC) (graphs in Fig. 3B.*i*' and B.*ii*'). They also exhibited fed hyperglycemia starting at 6–7 months of age (Tables 1 and S2). Like global *Cc1*$^{-/-}$ mice [11], *Alb+Cc1*$^{fl/fl}$ mutants maintained fasting euglycemia up to 8–9 months of age (Table S3), reflecting intact β-cell function and ruling out a defect in insulin secretion. This was supported by elevated C-peptide levels (Fig. 2A.*ii*), normal plasma glucagon levels (Tables 1, S2 and S3) and normal pancreatic proinsulin and proglucagon mRNA levels as compared to the controls (Table S4).

To further assess the effect of losing hepatic CEACAM1 on insulin action in vivo, a 2-h hyperinsulinemic-euglycemic clamp analysis was performed on overnight-fasted, awake 7-month-old *Alb+Cc1*$^{fl/fl}$ mice and all littermate controls (Fig. 4). The glucose infusion rate required to maintain euglycemia was lower in *Alb+Cc1*$^{fl/fl}$ mice (Fig. 4A), indicating insulin resistance in these mutants.

Insulin suppresses hepatic glucose production by inhibiting gluconeogenesis and stimulating net hepatic glucose uptake and subsequent glycogen synthesis [27]. Whole-body glycogen synthesis was intact in *Alb+Cc1*$^{fl/fl}$ mutants (Fig. 4B). Whereas pre-clamped basal (b) hepatic

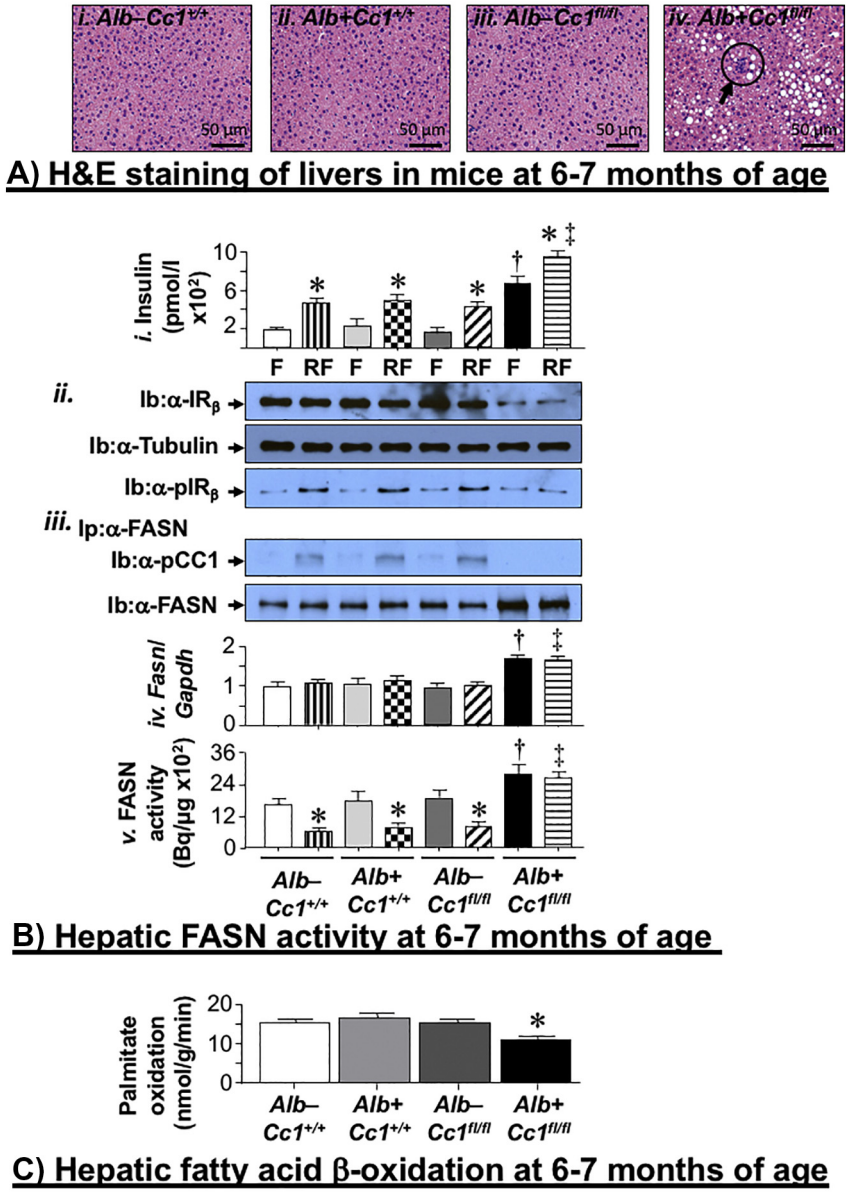

Fig. 5. Lipid metabolism in liver. (A) H&E staining in the liver of 6–7 month-old (*i*), *Alb–Cc1*$^{+/+}$, (*ii*), *Alb+Cc1*$^{+/+}$ (*iii*), *Alb–Cc1*$^{fl/fl}$, and (*iv*) *Alb+Cc1*$^{fl/fl}$ mice ($n = 5$/genotype). The circle in panel (*iv*) points to foci of inflammatory cell infiltrates. (B) Mice (6–7 months of age) were fasted overnight (F) and refed for 7 h (RF) and retro-orbital blood was removed to analyze (*i*) plasma insulin levels ($n = 6$/genotype/feeding state). Values are expressed as mean ± SEM. $^{*}P < 0.05$ refed vs fasted per genotype, $^{\dagger}P < 0.05$ *Alb+Cc1*$^{fl/fl}$ vs other genotypes at fasting, $^{\ddagger}P < 0.05$ *Alb+Cc1*$^{fl/fl}$ vs other genotypes at refeeding. (*ii*) Western blot analysis of liver lysates was carried out to assess insulin receptor protein level (α-IR$_{\beta}$) and phosphorylation (α-pIR$_{\beta}$). Immunoblotting with α-tubulin was used for normalization. (*iii*) Some aliquots were subjected to immunoprecipitation (Ip) with α-FASN antibody followed by immunoblotting (Ib) with α-pCEACAM1 antibody (α-pCC1). Gels represent two separate experiments performed on different mice/genotype/feeding state. (*iv*) *Fasn* mRNA expression relative to *Gapdh* was analyzed in triplicate by qRT-PCR ($n = 5$/genotype/feeding state; performed in triplicate). Values are expressed as mean ± SEM. $^{\dagger}P < 0.05$ *Alb+Cc1*$^{fl/fl}$ vs other genotypes at fasting, $^{\ddagger}P < 0.05$ *Alb+Cc1*$^{fl/fl}$ vs other genotypes at refeeding. (*v*) FASN activity was measured in triplicate by [^{14}C]-malonyl-CoA incorporation ($n = 5$/genotype/feeding state). Values are expressed as mean ± SEM. $^{\dagger}P < 0.05$ *Alb+Cc1*$^{fl/fl}$ vs other genotypes at fasting, $^{\ddagger}P < 0.05$ *Alb+Cc1*$^{fl/fl}$ vs other genotypes at refeeding. (C) Hepatic FAO (palmitate) in fasted 6–7 months of age mice, *Alb–Cc1*$^{+/+}$, (white bar), *Alb+Cc1*$^{+/+}$ (light grey bar), *Alb–Cc1*$^{fl/fl}$ (dark grey bar) and *Alb+Cc1*$^{fl/fl}$ (black bar) mice ($n = 5$/genotype). Assays were performed in triplicate. Values are expressed as mean ± SEM. $^{*}P < 0.05$ vs *Alb–Cc1*$^{+/+}$, *Alb+Cc1*$^{+/+}$ and *Alb–Cc1*$^{fl/fl}$.

glucose production, a measurement of the appearance rate (Ra), was normal in *Alb+Cc1*$^{fl/fl}$ mutants, insulin's ability to suppress hepatic glucose production (HGP) was compromised, as shown by higher hepatic glucose production during clamp (Fig. 4C) and reduced hepatic insulin action (Fig. 4D) in mutants relative to controls. In contrast, insulin-stimulated whole-body glucose turnover (R_d) was intact in 7-month-old *Alb+Cc1*$^{fl/fl}$ mice (Fig. 4E). This is consistent with intact glucose uptake in the gastrocnemius muscle (Fig. 4F), WAT (Fig. 4G) and brown adipose tissue (BAT) (Fig. 4H). Together, this suggests that *Alb+Cc1*$^{fl/fl}$ mice developed primarily hepatic insulin resistance at about 7 months of age.

3.4. *Alb+Cc1*$^{fl/fl}$ Mice Displayed Hepatic Fat Accumulation and Inflammation at 6–7 Months of Age

Hepatic triacylglycerol content was higher in *Alb+Cc1*$^{fl/fl}$ mice compared to the three controls starting at 6–7 months of age (Tables 1 and S2). Consistently, histological evaluation of H&E-stained liver sections revealed that unlike the three controls, *Alb+Cc1*$^{fl/fl}$ mice displayed diffused fat infiltration with both micro- and macro-steatosis at this age (Fig. 5A).

Hepatic steatosis could be due to high de novo lipogenesis and low fatty acid β-oxidation (FAO). The former was supported by elevated mRNA levels of hepatic genes involved in de novo lipogenesis (*Srebp1c* and *Fasn*) in mutant mice (Table S5). Because acute release of insulin represses FASN activity by inducing CEACAM1 phosphorylation and its binding to FASN [14], we refed mice (RF) for 7 h following an overnight fast (F) and assayed their FASN activity. Consistent with increased transcription of lipogenic genes by activated SREBP-1c under chronic hyperinsulinemia [9], basal (F) hepatic *Fasn* mRNA (Fig. 5B.*iv* and Table S5) and protein (Fig. 5B.*iii*) levels were higher in liver lysates of *Alb+Cc1*$^{fl/fl}$ relative to their three normo-insulinemic controls. Consequently, fasting FASN activity was higher in mutant than control mice (Fig. 5B.*v*). As expected from the acute negative effect of insulin on FASN activity under normo-insulinemic conditions [14], acute insulin release suppressed FASN activity in all controls (Fig. 5B.*v*; RF vs F). This was mediated by the ability of insulin to induce phosphorylation of the β-subunit of IR (pIR_β) (Fig. 5B.*ii*) and subsequently, CEACAM1 phosphorylation (pCC1) and its binding to FASN, as demonstrated by its detection in the α-FASN immunopellet (Fig. 5B.*iii*). In contrast, hyperinsulinemia drove insulin receptor downregulation in *Alb+Cc1*$^{fl/fl}$ mice, as shown by lower IR_β protein level than controls in the immunoblot of liver lysates with α-IR_β antibody (Fig. 5B.*ii*). This translated into restricted ability of insulin to induce IR_β phosphorylation (Fig. 5B.*ii*). Consistent with dependence on CEACAM1 phosphorylation for insulin to trigger CEACAM1/FASN interaction [14], pCC1 was not detected in the α-FASN immunopellet in mutant mice (Fig. 5B.*iii*). Consequently, insulin release failed to suppress FASN activity in the liver of refed relative to fasted *Alb+Cc1*$^{fl/fl}$, leading to increased hepatic lipogenesis in mutant mice.

Additionally, hepatic mRNA level of *Cpt1α*, a protein that transports fatty acids into mitochondria for FAO, was lower in *Alb+Cc1*$^{fl/fl}$ livers (Table S5). Consistently, FAO was reduced in *Alb+Cc1*$^{fl/fl}$ as shown by lower partial and total conversion of [$^{1\text{-}14}$C]-palmitate to CO_2 in mutant mice relative to controls (Fig. 5C).

H&E-stained sections of *Alb+Cc1*$^{fl/fl}$ mice showed multiple foci of inflammatory cell infiltrates in the hepatic lobules (Fig. 5A). This was supported by increased mRNA of *F4/80* (a marker of macrophage pool) and of other inflammatory markers such as hepatic tumor necrosis factor-α (*Tnfα*) and interleukin 6 (*Il-6*) (Table S5).

3.5. Increased Visceral Obesity in *Alb+Cc1*$^{fl/fl}$ Mice at 6–7 Months of Age

Consistent with increased redistribution of VLDL-triacylglycerol from liver to WAT, *Alb+Cc1*$^{fl/fl}$ mice developed visceral adiposity starting at 6–7 months of age (Tables 1 and S2). Despite loss of adiponectin (Table 1), this did not translate into insulin resistance in WAT at this age, as shown by intact glucose transport under hyperinsulinemic clamp conditions (Fig. 4G), intact insulin-stimulated Akt phosphorylation in refed (RF) relative to overnight-fasted (F) mice (Fig. 6A.*i*), and absence of lipolysis (as indicated by normal plasma NEFA (Table 1 and Fig. 6B.*i*) and mRNA levels of *Hsl* (Fig. 6C.*i*), the gene that encodes hormone-sensitive lipase, a key enzyme in lipolysis). In contrast, insulin resistance developed in WAT of mutant mice at 8–9 months of age, as supported by a blunted ability of insulin to induce Akt phosphorylation (Fig. 6A.*ii*), and the ~2-fold higher plasma NEFA (Fig. 6B.*ii*) and *Hsl* mRNA levels (Fig. 6C.*ii*). Thus, WAT of *Alb+Cc1*$^{fl/fl}$ mutants became insulin resistant at 8–9 months of age, releasing NEFA and contributing to sustained systemic insulin resistance [26,28].

3.6. *Alb+Cc1*$^{fl/fl}$ Mice Exhibited Energy Imbalance at 6–7 Months of Age

In addition to visceral adiposity, *Alb+Cc1*$^{fl/fl}$ mutants exhibited an increase in total fat mass with a reciprocal decrease in lean mass and consequently, increased total body weight starting at 6–7 months of age (Tables 1, S2 and S3).

To investigate whether altered fat distribution was associated with energy imbalance, we assessed daily food intake and subjected mice to indirect calorimetry. Relative to the three controls, *Alb+Cc1*$^{fl/fl}$ mutants displayed hyperphagia starting at 6–7 months of age (Figs. 7A

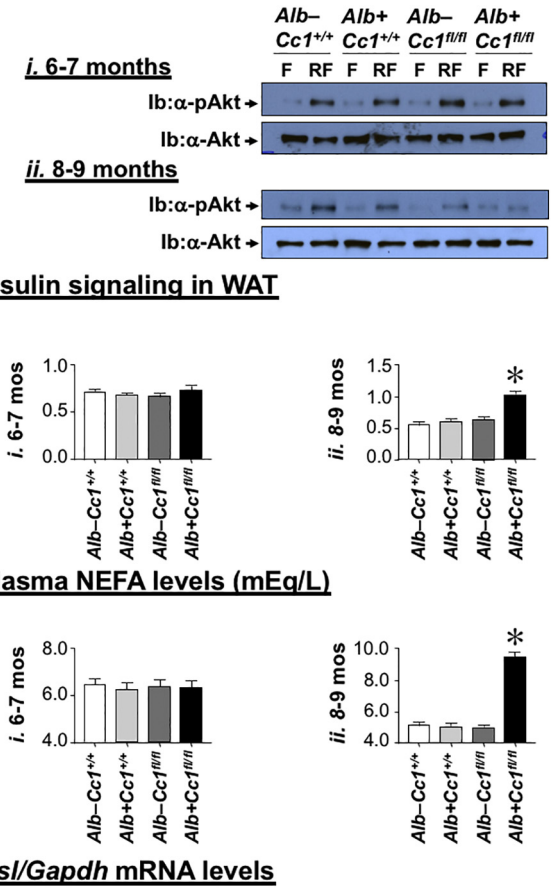

Fig. 6. Insulin signaling in white adipose tissue. (A) WAT was isolated from (*i*) 6–7 and (*ii*) 8–9 month-old fasted (F) and refed (RF) mice. Western analysis was performed by immunoblotting (Ib) with antibodies against phospho-Akt (α-pAkt), followed by α-Akt for normalization. Gels represent more than two separate experiments performed on different mice/genotype/treatment group. (B) Plasma NEFA levels were assayed in (*i*) 6–7 and (*ii*) 8–9 month-old overnight fasted mice [$n > 6$/each of *Alb–Cc1*$^{+/+}$ (white bar), *Alb+Cc1*$^{+/+}$ (light grey bar), *Alb–Cc1*$^{fl/fl}$ (dark grey bar) and *Alb+Cc1*$^{fl/fl}$ (black bar)]. (C) mRNA level of *Hsl* was analyzed by qRT-PCR relative to *Gapdh* in triplicate ($n = 5$/genotype). in (B and C), values are expressed as mean ± SEM. *$P < 0.05$ vs *Alb–Cc1*$^{+/+}$, *Alb+Cc1*$^{+/+}$ and *Alb–Cc1*$^{fl/fl}$.

and S2A). They also developed a marked decrease in total spontaneous physical activity at this age (Figs. 7B.*v* and S2B.*v*), including lower locomotor, ambulatory and standing activity (not shown). Like *Cc1*$^{-/-}$ mice [17], VO_2 consumption (Fig. 7B.*i*), CO_2 production (Fig. 7B.*ii*) and heat generation (Fig. 7B.*iv*) were not altered in *Alb*+*Cc1*$^{fl/fl}$ mutants.

3.7. Role of Hyperphagia in Systemic Insulin Resistance in Alb+Cc1$^{fl/fl}$ Mice

To test whether hyperphagia contributed to delayed systemic insulin resistance in *Alb*+*Cc1*$^{fl/fl}$, we subjected mutants at 7–8 months of age to a pair-feeding regimen to decrease their food intake and subsequently, lower their body mass [Fig. 8A.*i*; calorie restricted (CR) versus ad libitum (AL)-fed *Alb*+*Cc1*$^{fl/fl}$] to that of their AL-fed controls (Fig. 8A.*i*). As Fig. 8A.*ii* shows, caloric restriction restored tolerance to exogenous insulin in (CR)*Alb*+*Cc1*$^{fl/fl}$ mice. This indicates that hyperphagia contributed to systemic insulin resistance in older mutants.

3.8. Mechanisms of Energy Imbalance in Alb+Cc1$^{fl/fl}$ Mice

Consistent with increased visceral adiposity, hyperleptinemia was initiated at 6–7 months of age in *Alb*+*Cc1*$^{fl/fl}$ mice (Tables 1 and S2) in parallel to increased daily food intake (Fig. 7A). Hyperphagia could be caused at least partly, by blunted leptin signaling as shown by failure of intraperitoneally injected leptin to induce STAT3 phosphorylation (pSTAT3) in 7-month-old *Alb*+*Cc1*$^{fl/fl}$ like it did in their age-matched *Alb*–*Cc1*$^{fl/fl}$ controls (Fig. 9A).

Because hypothalamic FASN activation causes hyperphagia independently of leptin [29–31], we then examined FASN activity in the hypothalamus of 7-month-old mice. As in the liver (Fig. 5B), Western blot analysis revealed lower IR_{β} level in hypothalamic lysates of *Alb*+*Cc1*$^{fl/fl}$ relative to age-matched controls (Fig. 9B.*i*). Consistently, insulin release during refeeding (RF) failed to activate the insulin receptor in *Alb*+*Cc1*$^{fl/fl}$ hypothalami as it did in control mice [assessed by immunoblotting with phospho-IR_{β} antibody (α-pIR_{β})] (Fig. 9B.*i*, RF vs F). Insulin induced

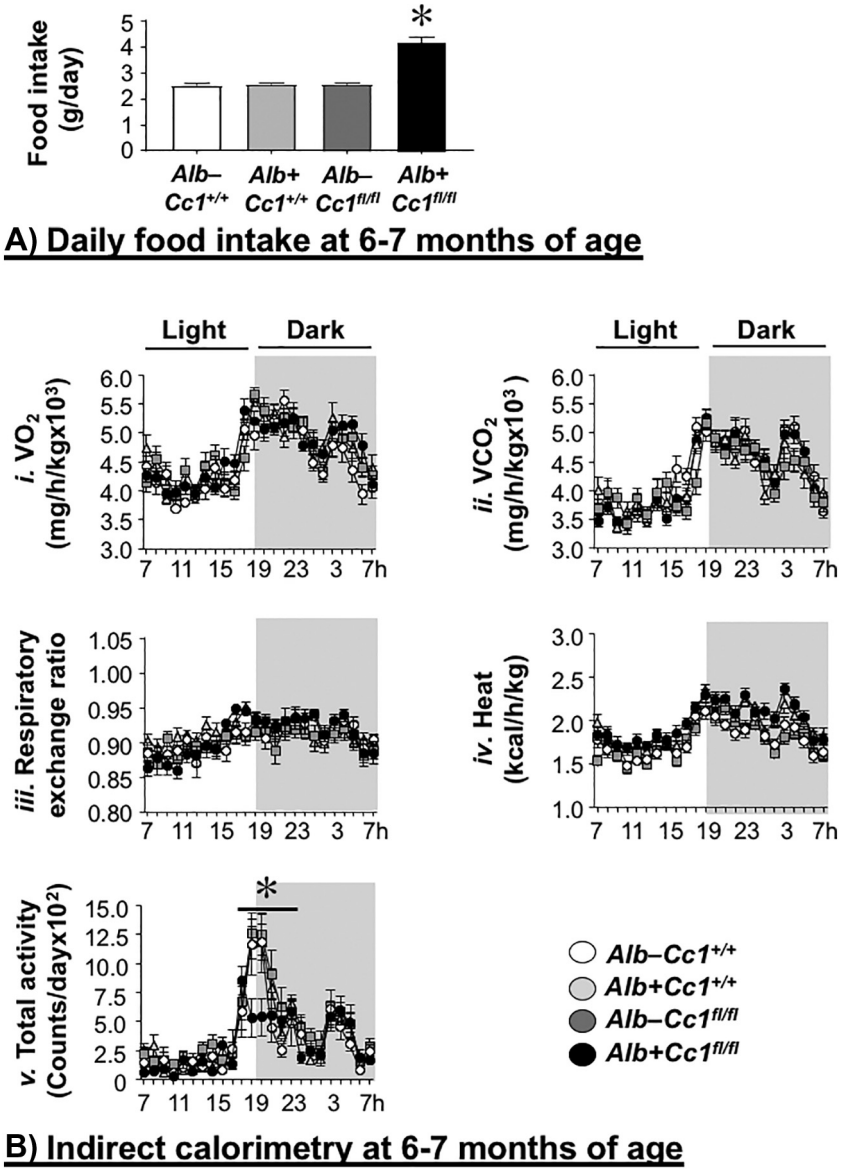

Fig. 7. Daily food intake and energy balance. (A) Daily food intake over 5 consecutive days was assessed on 6–7 months of age *Alb*–*Cc1*$^{+/+}$ (white bar), *Alb*+*Cc1*$^{+/+}$ (light grey bar), *Alb*–*Cc1*$^{fl/fl}$ (dark grey bar) and *Alb*+*Cc1*$^{fl/fl}$ (black bar) (n = 6/genotype). Values are expressed as mean ± SEM. *$P < 0.05$ vs *Alb*–*Cc1*$^{+/+}$, *Alb*+*Cc1*$^{+/+}$ and *Alb*–*Cc1*$^{fl/fl}$. (B) 6–7 month-old mice were individually caged ($n = 4$/genotype) and analyzed by indirect calorimetry (CLAMS system) for 5 days to measure (*i*) VO_2 consumption, (*ii*) VCO_2 production, (*iii*) respiratory exchange ratio, (*iv*) heat production, (*v*) calculated total activity every 20 min at a flow rate of 0.5 L/min for 24 h. Values are expressed as mean ± SEM of each time interval in the last 3 days in the light (07:00 h to 19:00 h) and dark (shaded; 19:00 h to 07:00 h) cycle. *$P < 0.05$ vs *Alb*–*Cc1*$^{+/+}$, *Alb*+*Cc1*$^{+/+}$ and *Alb*–*Cc1*$^{fl/fl}$.

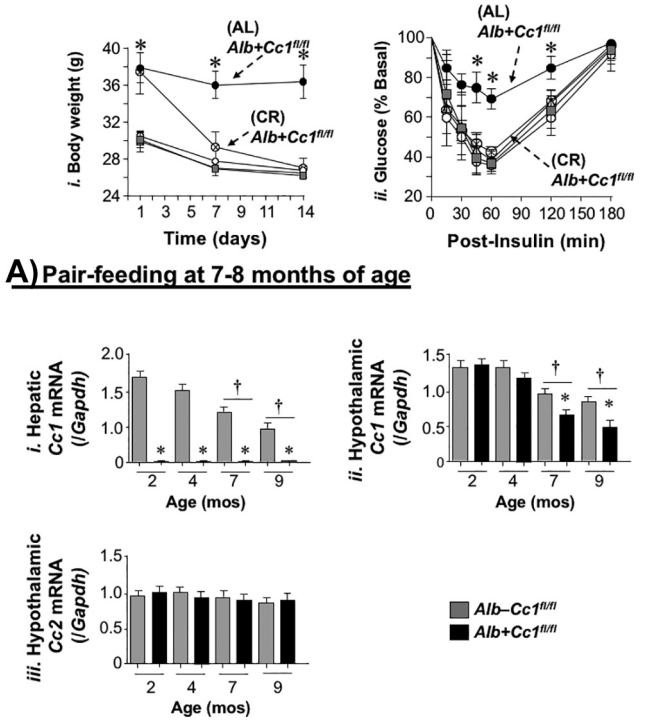

Fig. 8. Hyperphagia and systemic insulin resistance. (A) Pair-feeding experiments were performed on 7–8 month-old mice with some (***i***) *Alb+Cc1*$^{fl/fl}$ being fed ad libitum (AL) and others being subjected to caloric restriction (CR) for 2 weeks to decrease their body mass to the level of Ad libitum fed controls ($n = 6$/genotype/feeding group). (***ii***) At the end of the feeding period insulin tolerance was determined. (AL)*Alb–Cc1*$^{+/+}$ (white circle), (AL)*Alb+Cc1*$^{+/+}$ (light grey triangle), (AL)*Alb–Cc1*$^{fl/fl}$ (dark grey square), (AL)*Alb+Cc1*$^{fl/fl}$ (black circle) and (CR)*Alb+Cc1*$^{fl/fl}$ (hatched circle). Values are expressed as mean ± SEM at each time point. $^{*}P < 0.05$ vs (AL)*Alb–Cc1*$^{+/+}$, (AL)*Alb+Cc1*$^{+/+}$, (AL) *Alb–Cc1*$^{fl/fl}$ and (CR)*Alb+Cc1*$^{fl/fl}$. (B) *Ceacam1* (*Cc1*) mRNA content was analyzed by qRT-PCR in triplicate in liver (*i*) and hypothalamus (*ii*) of *Alb–Cc1*$^{fl/fl}$ (grey bar) and *Alb +Cc1*$^{fl/fl}$ (black bar) mice aged 2–9 months ($n = 5$/genotype/age group). (***iii***) *Cc2* mRNA was analyzed in the hypothalamus of *Alb–Cc1*$^{fl/fl}$ (grey bar) and *Alb+Cc1*$^{fl/fl}$ (black bar) mice aged 2–9 months, as in (*ii*). Values are expressed as mean ± SEM. $^{*}P < 0.05$ vs *Alb–Cc1*$^{fl/fl}$ of the same age group. $^{\dagger}P \le 0.05$ vs mice at the earliest age examined.

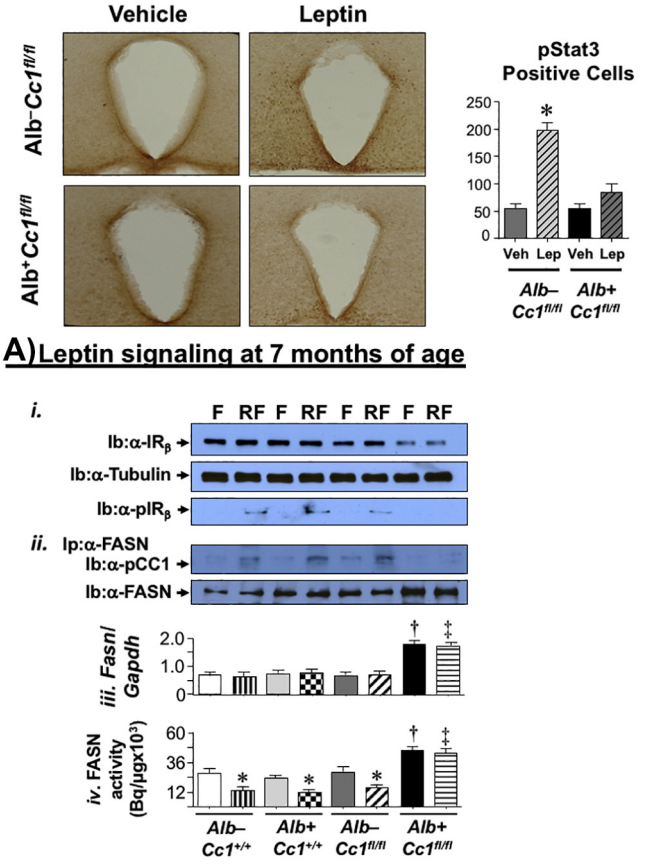

Fig. 9. Hypothalamic leptin signaling. (A) 7-month-old *Alb–Cc1*$^{fl/fl}$ and *Alb+Cc1*$^{fl/fl}$ mice (n = 5/treatment group) were injected intraperitoneally with vehicle (Veh, solid grey or black bars) or leptin (Lep, grey-and black-striped bars) 45 min prior to tissue isolation. Coronal sections from the medial hypothalamus were subjected to immunohistochemical analysis with phospho-STAT3 (pSTAT3) antibody. Values are presented as mean ± SEM of stained hypothalamic neurons of the medial hypothalamus. $^{*}P < 0.05$ vs vehicle/genotype. (B) Mice (7 months of age) were fasted overnight (F) and refed for 7 h (RF). (*i*) Western blot analysis investigating hypothalamic insulin receptor protein level (α-IRβ) and phosphorylation (α-pIRβ). α-tubulin was used to normalize IRβ against total loaded proteins. (*ii*) Some hypothalamic aliquots were used for immunoprecipitation (Ip) with α-FASN followed by immunoblotting (Ib) with α-pCEACAM1 antibody (α-pCC1). Gels represent two separate experiments performed on different mice/genotype/feeding state. (*iii*) *Fasn* mRNA expression was analyzed by qRT-PCR in triplicate relative to *Gapdh* ($n = 5$/genotype/feeding state). Values are expressed as mean ± SEM. $^{\dagger}P < 0.05$ *Alb+Cc1*$^{fl/fl}$ vs other genotypes at fasting, $^{\ddagger}P < 0.05$ *Alb+Cc1*$^{fl/fl}$ vs other genotypes at refeeding. (*iv*) FASN activity was measured in triplicate by [^{14}C]-malonyl-CoA incorporation ($n = 5$/genotype/feeding state). Values are expressed as mean ± SEM. $^{*}P < 0.05$ refed vs fasted/genotype, $^{\dagger}P < 0.05$ *Alb+Cc1*$^{fl/fl}$ vs other genotypes at fasting, $^{\ddagger}P < 0.05$ *Alb+Cc1*$^{fl/fl}$ vs other genotypes at refeeding.

CEACAM1 phosphorylation (pCC1) and detection in the FASN immunopellet in controls but not *Alb+Cc1*$^{fl/fl}$ mice (Fig. 9B.*ii*, RF vs F). This mediated a lower FASN activity in refed normo-insulinemic controls, but not in mutants in which chronic hyperinsulinemia drove higher basal mRNA (Fig. 9B.*iii*) and protein (Fig. 9B.*ii*) hypothalamic FASN levels and activity (Fig. 9B.*iv*), in parallel to a blunted ability of insulin to suppress FASN activity in refed mice (Fig. 9B.*iv*, RF vs F). Together with suppressed hypothalamic leptin signaling, hyperinsulinemia-driven defect in hypothalamic insulin signaling could contribute to hyperphagia to maintain progression of systemic insulin resistance in *Alb+Cc1*$^{fl/fl}$ mice.

CEACAM1 is expressed in the anorexigenic POMC neurons in the arcuate nucleus as well as in other hypothalamic neuronal populations [17]. Because insulin induces *Ceacam1* transcription [32], we then tested whether older *Alb+Cc1*$^{fl/fl}$ mutants exhibited lower hypothalamic *Ceacam1* levels resulting from systemic insulin resistance. As we have shown [33], *Ceacam1* mRNA level progressively decreased with age in wild-type livers (Fig. 8B.*i*). This cause a reduction in hepatic insulin clearance to compensate for age-related decrease in insulin secretion [34] and maintain insulin sensitivity in wild-type mice (Fig. 8B.*i*). Similarly, hypothalamic *Ceacam1* mRNA levels progressively declined, reaching ~30% loss in wild-type mice at 9 months, a level that does not compromise the regulatory effect of CEACAM1 on metabolism (Fig. 8B.*ii*). In the insulin-resistant mutants; however, the loss in hypothalamic *Ceacam1* mRNA levels reached at 9 months (Fig. 8B.*ii*) the 60% threshold that causes metabolic abnormalities [21]. In contrast, hypothalamic mRNA level of *Ceacam2*, a close relative to *Ceacam1* that is detected in neuropeptide Y-expressing neurons of the dorsomedial hypothalamus [35] and is involved in food intake suppression [22,36], was not altered with age (Fig. 8B.*iii*). The marked loss of CEACAM1 in hypothalamic POMC neurons and other hypothalamic neuronal populations could contribute to sustained energy imbalance and systemic insulin resistance in older *Alb+Cc1*$^{fl/fl}$ mutants.

4. Discussion

The cause-effect relationship between insulin resistance and hyperinsulinemia remains elusive [37]. Whereas primary insulin resistance causes hyperinsulinemia mainly by inducing a compensatory increase in insulin secretion [38], evidence in support of the causative role of chronic hyperinsulinemia in insulin resistance is mounting

[39,40], in particular when hyperinsulinemia results from impaired insulin clearance [41]. This is underlined by several mechanisms, including downregulation of the insulin receptor under hyperinsulinemic conditions [7,8]. This paradigm is bolstered by our previous findings that global deletion of *Ceacam1* gene impaired receptor-mediated insulin uptake and degradation to cause chronic hyperinsulinemia at the early age of 2 months, followed by downregulation of the insulin receptor and compromised insulin signaling in insulin target tissues to ultimately translate into insulin resistance, primarily hepatic, at about 6 months of age when the mutation was propagated onto the C57BL/6J background, as opposed to a mixed FVB background onto which insulin resistance developed concomitantly with hyperinsulinemia [11]. At 6 months of age, *C57BL/6J.Cc1*$^{-/-}$ mice also developed leptin resistance [17] and elevated lipolysis [11], but without any increase in β-cell mass [11], pointing to the relatively minor role of CEACAM1 in insulin secretion and ruling out a significant contribution by insulin secretion to hyperinsulinemia in global mutants. The current studies showed that liver-specific *AlbCre+Cc1*$^{fl/fl}$ null mice exhibited a stepwise progression of the pathogenesis of insulin resistance and altered lipid homeostasis. Liver-specific ablation of *Ceacam1* gene caused hyperinsulinemia at 2 months of age together with impaired insulin clearance when mice were propagated onto C57BL/6J background. This was not associated with any other metabolic derangement until 6–7 months of age, when insulin resistance, particularly hepatic, arose concomitantly with hepatic steatosis, visceral obesity, and compromised leptin signaling in association with energy imbalance (hyperphagia and reduced spontaneous physical activity). Hyperphagia caused progression to systemic insulin resistance, which became more pronounced at 8–9 months of age, as shown by impaired insulin signaling in WAT and elevated lipolysis. Absence of lipolysis until after hepatic insulin resistance developed in *AlbCre+Cc1*$^{fl/fl}$ nulls suggests that elevated plasma NEFA arose secondarily to chronic hyperinsulinemia which could cause insulin resistance in adipose tissue by reducing Glut4-mediated glucose transport [42], as supported by compromised insulin-stimulated Akt phosphorylation in WAT of the older *AlbCre+Cc1*$^{fl/fl}$ mutants. In addition, chronic hyperinsulinemia causes insulin resistance to the suppression of plasma NEFA levels and increasing de novo lipogenesis [43]. Given its lipotoxicity effect [28], elevated plasma NEFA could contribute to sustained systemic insulin resistance in older *AlbCre+Cc1*$^{fl/fl}$ mice [26]. This is consistent with the ability of L-Carnitine to ameliorate systemic insulin resistance in parallel to restoring plasma NEFA levels without directly affecting insulin degradation in L-SACC1 mice with liver-specific inactivation of *Ceacam1* [44].

Concomitantly with hepatic insulin resistance, *AlbCre+Cc1*$^{fl/fl}$ mice developed hepatic steatosis resulting from increased de novo lipogenesis and reduced fatty acid oxidation. Because the effect of CEACAM1 on FASN activity depends on the prior insulinemic state, it is likely that increased de novo lipogenesis primarily resulted from the hyperinsulinemic state caused by the loss of *Ceacam1* in liver. Nonetheless, hepatic steatosis was followed by redistribution of lipid substrates, preferentially to WAT, as expected from the C57BL/6J background [45], to cause visceral obesity. In addition to releasing NEFA, increase in visceral obesity caused a decrease in plasma adiponectin level with a reciprocal increase in leptin release. The former could contribute to sustained systemic insulin resistance in older *AlbCre+Cc1*$^{fl/fl}$ mice [46]. The latter could contribute to reduced hypothalamic STAT3 signaling in response to intraperitoneally injected leptin and hyperphagia [47], which in turn, caused systemic insulin resistance, as demonstrated by pair-feeding experiments.

Hyperphagia and reduced locomotor activity could be caused by hyperinsulinemia-driven systemic factors. By downregulating insulin receptors, hyperinsulinemia caused hypothalamic insulin resistance and restricted the ability of insulin to induce CEACAM1 phosphorylation and subsequently, suppress FASN activity. Because high hypothalamic FASN activity causes hyperphagia independently of leptin resistance [29,30], it is likely that hyperinsulinemia-driven hypothalamic insulin resistance caused hyperphagia, which in turn led to systemic insulin resistance in older *AlbCre+Cc1*$^{fl/fl}$ mice [48,49]. Consistent with hypothalamic insulin resistance being a main determinant of lipolysis [50], it preceded adipocytic insulin resistance and the rise in plasma NEFA in *AlbCre+Cc1*$^{fl/fl}$ mice. Thus, in addition to hepatic insulin resistance, chronic hyperinsulinemia drove hypothalamic insulin resistance, which could contribute to progressive systemic insulin resistance by causing hyperphagia and energy imbalance [49]. This central effect of chronic hyperinsulinemia agrees with our previous findings showing restoration of energy balance and all of the metabolic abnormalities by curbing hyperinsulinemia upon liver-specific rescuing of CEACAM1 [16].

Consistent with reduced insulin clearance with aging [4], the current as well as our previous studies [33], showed that hepatic CEACAM1 expression progressively decreased with age in wild-type mice, likely to compensate for the age-related decline in insulin secretion [34] in order to maintain physiologic insulin homeostasis and action. Similarly, hypothalamic *Ceacam1* mRNA levels progressively decreased with age in wild-type mice, but by ~35%, which would not cause a significant metabolic abnormality, as expected from the normal phenotype in heterozygous global *Cc1*$^{+/-}$ mice [11]. In *AlbCre+Cc1*$^{fl/fl}$ mice; however, the age-related loss of hypothalamic *Ceacam1* mRNA reached ≥60% at 9 months of age, likely stemming from the parallel progression of systemic insulin resistance and resultant loss of transcriptional upregulation by insulin [32]. Because CEACAM1 is expressed in POMC and other hypothalamic neurons [17] that control energy balance, its age-related significant reduction in this neuronal population could contribute to energy imbalance, and subsequently, to sustained insulin resistance by inducing lipolysis in older *AlbCre+Cc1*$^{fl/fl}$ mutants [50]. This hypothesis must await further studies, including deleting *Ceacam1* gene in POMC neurons, to be tested.

In summary, our data demonstrated that liver-specific deletion of *Ceacam1* primarily caused chronic hyperinsulinemia resulting from impaired insulin clearance, and that this led to hepatic insulin resistance and steatosis, and to hypothalamic insulin resistance, which by triggering energy imbalance, mediated the progression of systemic insulin resistance and altered hypothalamic control of lipolysis that in turn, contributed to sustained systemic insulin resistance in older mice. The earlier onset of hyperinsulinemia and impaired insulin clearance than hepatic insulin resistance followed by lipolysis in this liver-specific loss-of-function *AlbCre+Cc1*$^{fl/fl}$ model provided an in vivo demonstration that chronic hyperinsulinemia resulting primarily from impaired insulin clearance can cause secondary hepatic insulin resistance independently of lipolysis. Moreover, by causing hypothalamic insulin resistance, hyperinsulinemia can lead to energy imbalance and progressive systemic insulin resistance.

Supplementary data to this article can be found online at https://doi.org/10.1016/j.metabol.2019.01.008.

Acknowledgments

We thank M. Kopfman at the Najjar laboratory for her technical assistance in maintaining the mouse lines and assisting in genotyping and phenotyping. We also thank the Osteopathic Heritage Foundation for its John J. Kopchick, PhD, Eminent Research Chair fund to SMN.

Funding

This work was supported by NIH grants: R01-DK054254, R01-DK083850, and R01-HL112248 to SMN, R01-HD081792 to JWH, and 5U2C-DK093000 to JKK. The work was also supported by the Middle-East Diabetes Research Center to HEG and SSG, and the American Heart Association (14POST20480294) to LR.

Duality of Interest

The authors declare no duality of interest.

Author Contributions

HEG, LR, HTM, SSG, IHM, JEH, HLN, and SS researched data. HEG coordinated the research among co-authors, analyzed data and wrote the first draft of the manuscript. JKK analyzed the hyperinsulinemic-euglycemic clamp data. SMN analyzed data and reviewed and revised the manuscript. SMN had full access to all the data of the study and takes responsibility for the conception of the studies and for the integrity and accuracy of data analysis. Original data are available upon request from the senior author.

References

[1] Polidori DC, Bergman RN, Chung ST, Sumner AE. Hepatic and extrahepatic insulin clearance are differentially regulated: results from a novel model-based analysis of intravenous glucose tolerance data. Diabetes 2016;65:1556–64.
[2] Matveyenko AV, Liuwantara D, Gurlo T, Kirakossian D, Dalla Man C, Cobelli C, et al. Pulsatile portal vein insulin delivery enhances hepatic insulin action and signaling. Diabetes 2012;61:2269–79.
[3] Porksen N, Munn S, Steers J, Vore S, Veldhuis J, Butler P. Pulsatile insulin secretion accounts for 70% of total insulin secretion during fasting. Am J Physiol Endocrinol Metab 1995;269:E478–88.
[4] Mohamad M, Mitchell SJ, Wu LE, White MY, Cordwell SJ, Mach J, et al. Ultrastructure of the liver microcirculation influences hepatic and systemic insulin activity and provides a mechanism for age-related insulin resistance. Aging Cell 2016;15:706–15.
[5] Tokarz VL, MacDonald PE, Klip A. The cell biology of systemic insulin function. J Cell Biol 2018;217:2273–89.
[6] Ward GM, Walters JM, Aitken PM, Best JD, Alford FP. Effects of prolonged pulsatile hyperinsulinemia in humans. Enhancement of insulin sensitivity. Diabetes 1990; 39:501–7.
[7] Flier JS. Insulin receptors and insulin resistance. Annu Rev Med 1983;34:145–60.
[8] Knutson VP, Ronnett GV, Lane MD. Rapid, reversible internalization of cell surface insulin receptors. Correlation with insulin-induced down-regulation. J Biol Chem 1983;258:12139–42.
[9] Horton JD, Goldstein JL, Brown MS. SREBPs: activators of the complete program of cholesterol and fatty acid synthesis in the liver. J Clin Invest 2002;109:1125–31.
[10] Poy MN, Yang Y, Rezaei K, Fernstrom MA, Lee AD, Kido Y, et al. CEACAM1 regulates insulin clearance in liver. Nat Genet 2002;30:270–6.
[11] DeAngelis AM, Heinrich G, Dai T, Bowman TA, Patel PR, Lee SJ, et al. Carcinoembryonic antigen-related cell adhesion molecule 1: a link between insulin and lipid metabolism. Diabetes 2008;57:2296–303.
[12] Choice CV, Howard MJ, Poy MN, Hankin MH, Najjar SM. Insulin stimulates pp 120 endocytosis in cells co-expressing insulin receptors. J Biol Chem 1998;273: 22194–200.
[13] Choice CV, Poy MN, Formisano P, Najjar SM. Comparison of the intracellular trafficking of two alternatively spliced isoforms of pp120, a substrate of the insulin receptor tyrosine kinase. J Cell Biochem 1999;76:133–42.
[14] Najjar SM, Yang Y, Fernstrom MA, Lee SJ, Deangelis AM, Rjaily GA, et al. Insulin acutely decreases hepatic fatty acid synthase activity. Cell Metab 2005;2:43–53.
[15] Kabir M, Catalano KJ, Ananthnarayan S, Kim SP, Van Citters GW, Dea MK, et al. Molecular evidence supporting the portal theory: a causative link between visceral adiposity and hepatic insulin resistance. Am J Physiol Endocrinol Metab 2005;288:E454–61.
[16] Russo L, Muturi HT, Ghadieh HE, Ghanem SS, Bowman TA, Noh HL, et al. Liver-specific reconstitution of CEACAM1 reverses the metabolic abnormalities caused by its global deletion in male mice. Diabetologia 2017;60:2463–74.
[17] Heinrich G, Russo L, Castaneda TR, Pfeiffer V, Ghadieh HE, Ghanem SS, et al. Leptin resistance contributes to obesity in mice with null mutation of carcinoembryonic antigen-related cell adhesion molecule 1. J Biol Chem 2016;291:11124–32.
[18] Nagaishi T, Pao L, Lin SH, Iijima H, Kaser A, Qiao SW, et al. SHP1 phosphatase-dependent T cell inhibition by CEACAM1 adhesion molecule isoforms. Immunity 2006;25:769–81.
[19] Najjar SM, Philippe N, Suzuki Y, Ignacio GA, Formisano P, Accili D, et al. Insulin-stimulated phosphorylation of recombinant pp120/HA4, an endogenous substrate of the insulin receptor tyrosine kinase. Biochemistry 1995;34:9341–9.
[20] Najjar SM, Ledford KJ, Abdallah SL, Paus A, Russo L, Kaw MK, et al. Ceacam1 deletion causes vascular alterations in large vessels. Am J Physiol Endocrinol Metab 2013; 305:E519–29.
[21] Al-Share QY, DeAngelis AM, Lester SG, Bowman TA, Ramakrishnan SK, Abdallah SL, et al. Forced hepatic overexpression of CEACAM1 curtails diet-induced insulin resistance. Diabetes 2015;64:2780–90.
[22] Heinrich G, Ghosh S, Deangelis AM, Schroeder-Gloeckler JM, Patel PR, Castaneda TR, et al. Carcinoembryonic antigen-related cell adhesion molecule 2 controls energy balance and peripheral insulin action in mice. Gastroenterology 2010; 139:644–52.
[23] Geissmann Q. OpenCFU, a new free and open-source software to count cell colonies and other circular objects. PLoS One 2013;8:e54072.
[24] Houde C, Roy S, Leung N, Nicholson DW, Beauchemin N. The cell adhesion molecule CEACAM1-L is a substrate of caspase-3-mediated cleavage in apoptotic mouse intestinal cells. J Biol Chem 2003;278:16929–35.
[25] Ramakrishnan SK, Russo L, Ghanem SS, Patel PR, Oyarce AM, Heinrich G, et al. Fenofibrate decreases insulin clearance and insulin secretion to maintain insulin sensitivity. J Biol Chem 2016;291:23915–24.
[26] Pereira S, Park E, Mori Y, Haber CA, Han P, Uchida T, et al. FFA-induced hepatic insulin resistance in vivo is mediated by PKCδ, NADPH oxidase, and oxidative stress. Am J Physiol Endocrinol Metab 2014;307:E34–46.
[27] DeFronzo RA. Lilly lecture 1987. The triumvirate: beta-cell, muscle, liver. A collusion responsible for NIDDM. Diabetes 1988;37:667–87.
[28] Bergman RN, Kim SP, Catalano KJ, Hsu IR, Chiu JD, Kabir M, et al. Why visceral fat is bad: mechanisms of the metabolic syndrome. Obesity (Silver Spring) 2006;14 (Suppl. 1):16S–9S.
[29] Shimokawa T, Kumar MV, Lane MD. Effect of a fatty acid synthase inhibitor on food intake and expression of hypothalamic neuropeptides. Proc Natl Acad Sci U S A 2002;99:66–71.
[30] Mobbs CV, Makimura H. Block the FAS, lose the fat. Nat Med 2002;8:335–6.
[31] Kumar MV, Shimokawa T, Nagy TR, Lane MD. Differential effects of a centrally acting fatty acid synthase inhibitor in lean and obese mice. Proc Natl Acad Sci U S A 2002; 99:1921–5.
[32] Najjar S, Boisclair Y, Nabih Z, Philippe N, Imai Y, Suzuki Y, et al. Cloning and characterization of a functional promoter of the rat pp120 gene, encoding a substrate of the insulin receptor tyrosine kinase. J Biol Chem 1996;271:8809–17.
[33] Ghanem SS, Muturi HT, DeAngelis AM, Hu J, Kulkarni RN, Heinrich G, et al. Age-dependent insulin resistance in male mice with null deletion of the carcinoembryonic antigen-related cell adhesion molecule 2 gene. Diabetologia 2017;60:1751–60.
[34] Westacott MJ, Farnsworth NL, St Clair JR, Poffenberger G, Heintz A, Ludin NW, et al. Age-dependent decline in the coordinated [Ca(2+)] and insulin secretory dynamics in human pancreatic islets. Diabetes 2017;66:2436–45.
[35] Draper S, Kirigiti M, Glavas M, Grayson B, Chong CN, Jiang B, et al. Differential gene expression between neuropeptide Y expressing neurons of the dorsomedial nucleus of the hypothalamus and the arcuate nucleus: microarray analysis study. Brain Res 2010;1350:139–50.
[36] Patel PR, Ramakrishnan SK, Kaw MK, Raphael CK, Ghosh S, Marino JS, et al. Increased metabolic rate and insulin sensitivity in male mice lacking the carcino-embryonic antigen-related cell adhesion molecule 2. Diabetologia 2012;55:763–72.
[37] Shanik MH, Xu Y, Skrha J, Dankner R, Zick Y, Roth J. Insulin resistance and hyperinsulinemia: is hyperinsulinemia the cart or the horse? Diabetes Care 2008; 31(Suppl. 2):S262–8.
[38] Ferrannini E. The stunned beta cell: a brief history. Cell Metab 2010;11:349–52.
[39] Corkey BE. Banting lecture 2011: hyperinsulinemia: cause or consequence? Diabetes 2012;61:4–13.
[40] Pories WJ, Dohm GL. Diabetes: have we got it all wrong? Hyperinsulinism as the culprit: surgery provides the evidence. Diabetes Care 2012;35:2438–42.
[41] Ader M, Stefanovski D, Kim SP, Richey JM, Ionut V, Catalano KJ, et al. Hepatic insulin clearance is the primary determinant of insulin sensitivity in the normal dog. Obesity (Silver Spring) 2014;22:1238–45.
[42] Gonzalez E, Flier E, Molle D, Accili D, McGraw TE. Hyperinsulinemia leads to uncoupled insulin regulation of the GLUT4 glucose transporter and the FoxO1 transcription factor. Proc Natl Acad Sci U S A 2011;108:10162–7.
[43] Koopmans SJ, Kushwaha RS, DeFronzo RA. Chronic physiologic hyperinsulinemia impairs suppression of plasma free fatty acids and increases de novo lipogenesis but does not cause dyslipidemia in conscious normal rats. Metabolism 1999;48:330–7.
[44] Dai T, Abou-Rjaily GA, Al-Share QY, Yang Y, Fernstrom MA, Deangelis AM, et al. Interaction between altered insulin and lipid metabolism in CEACAM1-inactive transgenic mice. J Biol Chem 2004;279:45155–61.
[45] Haluzik M, Colombo C, Gavrilova O, Chua S, Wolf N, Chen M, et al. Genetic background (C57BL/6J versus FVB/N) strongly influences the severity of diabetes and insulin resistance in Ob/Ob mice. Endocrinology 2004;145:3258–64.
[46] Turer AT, Scherer PE. Adiponectin: mechanistic insights and clinical implications. Diabetologia 2012;55:2319–26.
[47] Bjorbaek C. Central leptin receptor action and resistance in obesity. J Invest Med 2009;57:789–94.
[48] Woods SC, Lotter EC, McKay LD, Porte Jr D. Chronic intracerebroventricular infusion of insulin reduces food intake and body weight of baboons. Nature 1979;282:503–5.
[49] Schwartz MW, Woods SC, Porte Jr D, Seeley RJ, Baskin DG. Central nervous system control of food intake. Nature 2000;404:661–71.
[50] Shin AC, Filatova N, Lindtner C, Chi T, Degann S, Oberlin D, et al. Insulin receptor signaling in POMC, but not AgRP, neurons controls adipose tissue insulin action. Diabetes 2017;66:1560–71.